


# Exploring 3D printing techniques for the hybrid fabrication of discrete topology optimized structures

International Journal of  
Architectural Computing  
2021, Vol. 0(0) 1–20  
© The Author(s) 2021  
Article reuse guidelines:  
[sagepub.com/journals-permissions](https://sagepub.com/journals-permissions)  
DOI: 10.1177/14780771211039084  
[journals.sagepub.com/home/jac](https://journals.sagepub.com/home/jac)  


Mauricio Morales-Beltran<sup>1</sup> , Berk Selamoğlu<sup>1</sup>, Kaan Çetin<sup>1</sup>,  
Halis Arda Özdemir<sup>1</sup> and Fulya Özbey<sup>2</sup>

## Abstract

The application of topology optimization methods in architecture, while useful for conceptual design explorations, seems to be limited by the practical realization of continuum-type design outcomes. One way to overcome this limitation is setting up design and fabrication techniques, through which continuum domains become discrete structures. This study investigates to which extent discrete optimized systems can be built using a hybrid approach combining 3D printing and analogue fabrication techniques. The procedure is based on an algorithm in Grasshopper (Rhinoceros) that translates continuum topologies obtained in MATLAB into discrete systems, providing alternatives depending on the targeted volume fraction, the intended surface smoothness of the structural components and building material. The study focuses on fabrication aspects and structural performance of discrete structures using 3D printed nodes. Experimental tests evaluate the compressive strength of different types of filaments with varied infill percentages. Final prototypes are fabricated using a hybrid technique involving the use of 3D printed nodes to assemble bar-arrays comprising wooden members. Results provide a critical appraisal of the limitations and potentialities of 3D printing for hybrid fabrication of real scale structures.

## Keywords

Topology optimization, discrete structures, material hybridity, digital fabrication, conceptual design, PLA, PETG

## Introduction

Topology optimization can be defined as a group of methods aiming at finding the optimal layout of either continuum-type structures or grid-type structures, also known as discrete systems.<sup>1</sup> Continuum topology

---

<sup>1</sup>Department of Architecture, Faculty of Architecture, Yaşar University, Izmir, Turkey

<sup>2</sup>Department of Interior Architecture, Faculty of Architecture, Yaşar University, Izmir, Turkey

### Corresponding author:

Mauricio Morales-Beltran, Department of Architecture, Faculty of Architecture, Yasar University, Universite Caddesi No. 37-39, Bornova 35100, Izmir, Turkey.

Email: [mauricio.morales-beltran@yasar.edu.tr](mailto:mauricio.morales-beltran@yasar.edu.tr)

optimization is the process of determining the optimal layout of material distribution, that is, the shape of the holes and connectivity, inside a given design domain.<sup>2</sup> Discrete procedures aim at finding the optimal layouts of structures comprising bar or beam elements through the sizing of members and/or shaping the definition of nodes and elements connectivity.

Continuum procedures allow designers for greater design freedom than size and shape optimization of discrete systems as the latter ones deal with predefined structural configurations.<sup>3</sup> The use of continuum topology optimization has been addressed as a means to explore emerging typologies and to open up new shape possibilities, especially during the early conceptual design and preliminary design phases.<sup>3-7</sup> However, there are some conceptual shortcomings when dealing with topology optimization in architecture:

- The use of currently available methods, based on homogeneous materials displaying linear elastic behaviour, leads to unnecessary complexities when heterogeneous materials are used, simultaneously restricting their potential for further design explorations;<sup>5</sup>
- Given both the lack of an explicit description of the structure and that the resulting density field is expressed by numerical values between one and zero, there is a large number of intermediate densities that are difficult to interpret in the final result. This may also cause the loss of optimality for the final shape;<sup>8</sup>
- Control of the design in topology optimization is only possible by indirect measures, for example, support conditions, design domain geometry, etc., which makes the entire process impractical to conventional design practice;<sup>5</sup> and
- Architectural design – as often driven by creativity, inspiration, and aesthetics – cannot easily be framed within a mathematical formulation, so designer's choices in optimization are reduced to mechanical inputs. A major correlated setback is that a particular design is no longer unique as anyone making similar choices could easily obtain similar optimization results.<sup>8</sup>

In addition, the application of these methods in architecture seems to be limited, mostly, by the practical realization of the obtained results. Most of the available methods deal with continuum design domains, whose results cannot be translated directly into architecture structures using discrete elements, that is, beams, columns and plates. In practice, the outcomes of continuum procedures still require a laborious, time-consuming, post-optimization geometric rationalization of results, necessary for translating optimized shapes into buildable discrete geometry.<sup>3,5,8</sup>

In order to streamline the transition from conceptual topology optimization to further stages of design, analysis and fabrication, researchers have suggested a closer coupling between optimization and fabrication procedures,<sup>5,9</sup> and the search for algorithms that can identify engineering features in topology results, such as fillets, extrusions, planes and beam sections among others.<sup>3</sup> Combined continuum and discrete optimization procedures have been already proposed not only for considering the production of structures<sup>4</sup> but also to solve design limitations associated to the use of continuum methods. For example, in the optimal design of braced frames for high-rise applications,<sup>6</sup> a combination of discrete and continuum elements is proposed to overcome the high concentration of material toward the edges of the domain.

With the advent of additive manufacturing (AM), the possibilities of digitally fabricating these non-standard shapes have increased substantially. This possibility, however, is obtained at the expenses of customized and often time-consuming fabrication settings, raising the need of researching on means to produce these continuum structures using regular and affordable 3D printers. The main disadvantage, however, is that the use of fused filament fabrication (FFF) techniques will result in 3D printed parts exhibiting 'inferior mechanical performance to parts fabricated using conventional polymer processing technologies, such as compression moulding'<sup>10</sup> because the mechanical strength of 3D printed components is direction-dependant.<sup>10-14</sup> Thus, to enhance the structural strength of the printed polymer components,

techniques such as adding fibres to the polymer matrix,<sup>10,15</sup> changing the printing angle<sup>11</sup> and regulating the polymer viscosity by controlling the printing temperature<sup>12</sup> have been proposed. The reason behind the wide use of 3D printing techniques lies in its potential for using different materials and composites, the possibility to produce small- to large-scale prototypes and its easiness to operate and be modified.<sup>13</sup>

In the case of fabricating topology optimized systems, instead of printing the whole structure, parts would be printed separately and further assembled. Furthermore, the transformation from continua to discrete systems opens up the possibility of turning some of the discrete components into regular section bars. By using standard linear components, for example, timber battens or steel profiles, only the connecting zones will be 3D printed as they would remain as in the original continuum design. The main advantages of this approach are that (a) varied sizes of standard components can be used, increasing flexibility of the design and (b) that each remaining continuum component can be printed in an orientation which maximizes its mechanical strength, from a layer deposition perspective.<sup>16</sup> However, this approach requires finding a design method accounting not only for the conversion from a 3D printed continuum system to a discrete one but also considering the conversion of irregular bars to be printed with polylactic acid (PLA) or polyethylene terephthalate glycol (PETG) filaments into equivalent regular bars made of a different material. In short, a method that accounts for a hybrid use of materials, for example, timber battens connected by nodes made of PLA or PETG. Here, the concept of hybridity not only expresses multi-materiality but also implies the use of varied digital fabrication methods.<sup>17</sup>

This study explores the use of topology optimization techniques in the design and fabrication of discrete structures and investigates to which extent these optimized systems can be built using a hybrid approach combining 3D printing and analogue fabrication techniques. The first part of the study provides a method to convert continuum topologies obtained in MATLAB,<sup>18</sup> into discrete systems using a complementary parametric routine hosted in Rhino-Grasshopper (GH) visual scripting interface.<sup>19</sup> The algorithm provides alternatives for the discrete designs depending on the targeted volume fraction and the intended surface smoothness of the structural components. The design procedure includes the conversion of bar-like members from the continuum systems, likely to be 3D printed, into bars with constant cross-sections made of different materials. The second part of the study provides an experimental assessment of 3D printed components of soon-to-be discrete structures. Although the mechanical strength of pieces produced with common printing filaments (PLA, PLA+ and PETG), and featuring varied infill densities have been investigated, studies mostly focus on tensile strength of PLA and acrylonitrile butadiene styrene (ABS) pieces. Fernandez-Vicente et al.<sup>14</sup> provide experimental testing showing that the change in infill density mainly determines the tensile strength of FFF 3D printed pieces. Their study also includes several examples of previous literature where infill, shell perimeters and layer height have been previously tested in both PLA and ABS. Infill density aside, other sources also address air-gaps, interfacial bonding and layer height as critical parameters affecting the mechanical behaviour of 3DP parts.<sup>15,20-22</sup> While most of the studies address the influence of infill patterns under tension and bending,<sup>15</sup> compression tests are seldom in research. For example, Ahn et al. reported that the printing direction was the only parameter evaluated in the compression tests 'because the complexity of test increases with more parameters'.<sup>15</sup> The research of Mazzanti et al.<sup>15</sup> establishes that many drawbacks associated to FFF 3D printing with both PLA and ABS 'could be controlled by carefully choosing the processing parameters'. However, the authors point out that given the large number of variables (layer thickness, infill geometry, infill density, number of layers, raster angle, raster gap and width and patterning), 'it is difficult to pinpoint the ones that mostly affect structure/properties correlations'. For this reason, experimental testing with PLA+ and PETG pieces was conducted to determine the shear strength of different anchoring systems and the compressive strength of different type of filaments combined with variations of infill percentages. Finally, cantilever prototypes are fabricated using a hybrid technique involving the use of PETG nodes to be further assembled in arrays comprising wooden members. These experiments and prototypes provided insights for the practical

realization of selected continuum designs using 3D printed nodes connecting commercially available discrete members.

## From continuum to discrete systems

The method to convert continuum topologies obtained in MATLAB into discrete systems is based on a parametric algorithm hosted in GH (Figure 1). The algorithm's main purpose is providing alternatives for the discrete designs including the conversion of bar-like members from the continuum systems into bars with constant cross-sections made of different materials.

### Continuum topology optimization

The procedure begins with the obtention of a continuum topology optimized solution from a numerical problem, which is defined in MATLAB. The topology optimization procedure is based on the 169-line code developed by Liu and Tovar,<sup>23</sup> which uses a density-based approach to solve a minimum compliance problem for three-dimensional design domains, for example, cantilevered and MBB beams. The selection of this code is based on that it requires few changes to modify boundary and loading conditions, and its implementation is straightforward as the design domain is simply defined in terms of  $nelx$ ,  $nely$  and  $nelz$ , that is, the number of

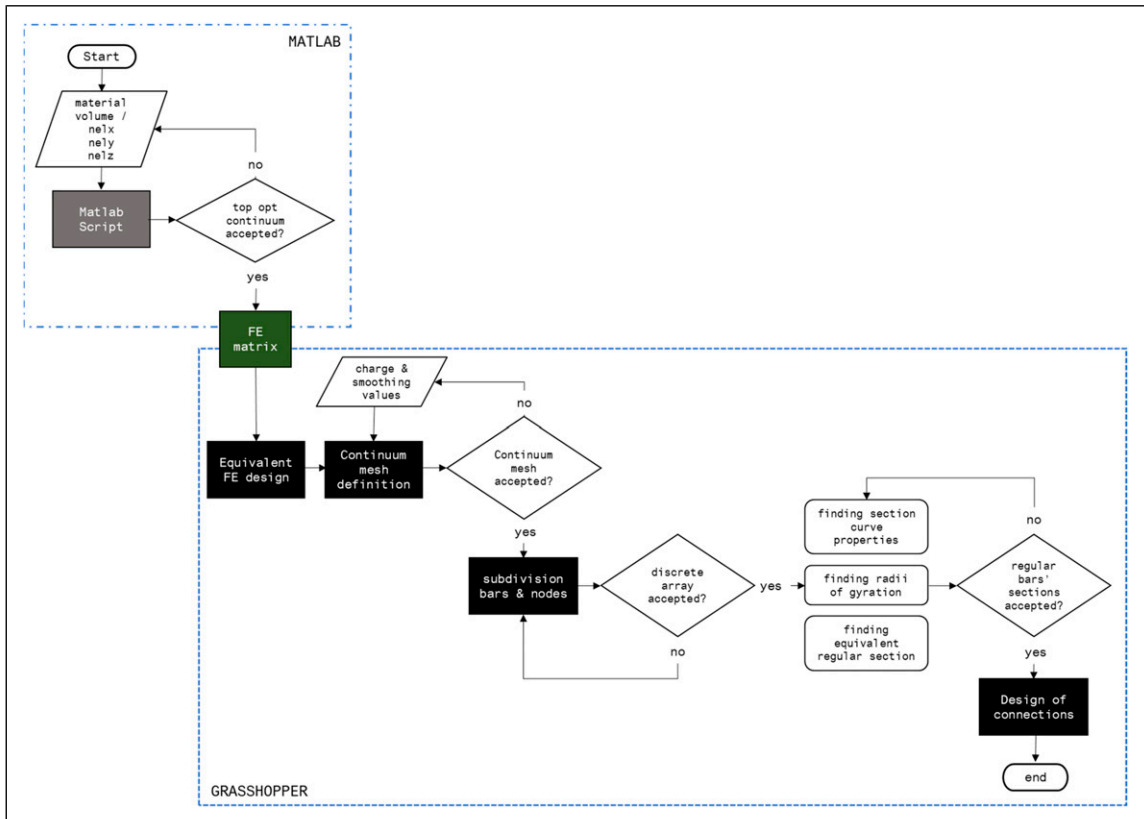
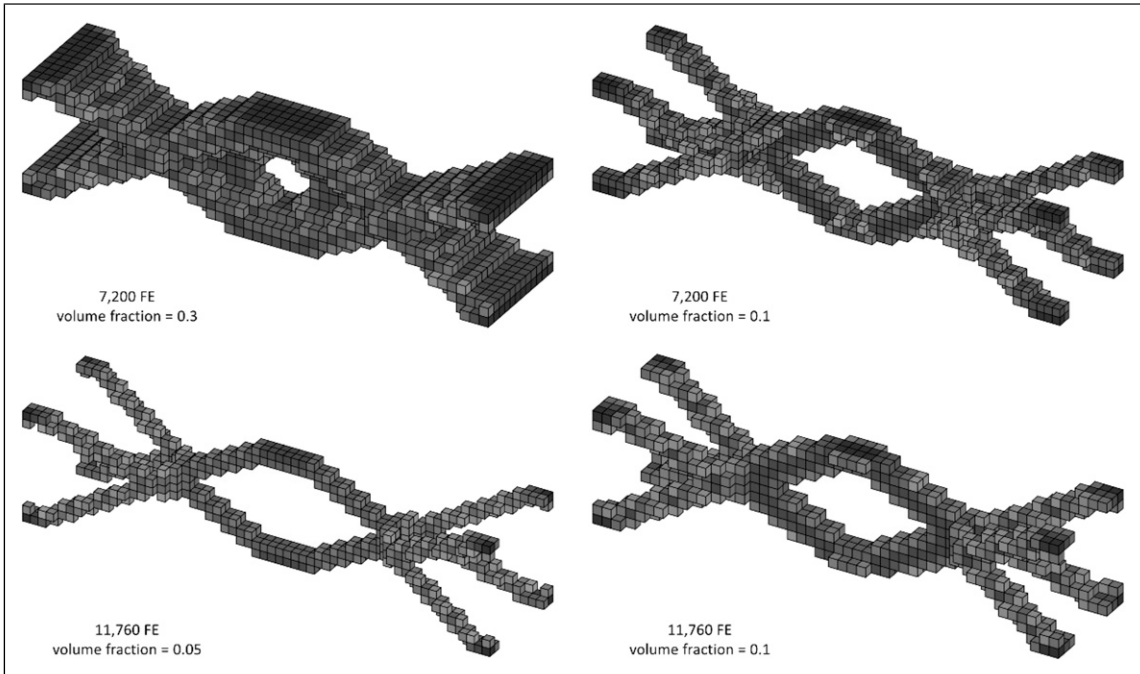


Figure 1. Flowchart of the procedure.



**Figure 2.** Influence of the number of FE and targeted volume fraction on the continua resulting from the topology optimization of a fixed beam loaded midspan.

elements in  $x$ ,  $y$  and  $z$  axes, respectively. The implemented code also includes an iterative solver, which allows solving problems with large finite element (FE) meshes. Large FE meshes are required to produce smoother continuum shapes that will not only be easier to convert to discrete structures but also that display larger reductions of material (Figure 2).

### *Reinterpretation of the continuum system in Grasshopper*

Previous to the definition of the discrete structures, the continuum optimizations from MATLAB must be imported into GH. A few lines were added to the original MATLAB code, allowing to export the three-dimensional array as an Excel file. Given the size limitations, the Cartesian axis containing the smaller number of FE (usually  $nely$ ) is taken as the total number of spreadsheets in the file, while the remaining two were taken as number of rows and columns in each of those spreadsheets. Based on this information, a two-step procedure is set up.

*Step 1: Creation of an equivalent finite element design.* In GH, the information contained in the spreadsheets is used to produce first an equivalent prismatic design domain containing  $nelx*nely*nely$  boxes with a density equals to one unit (Figure 3(a)). Next, using an Excel reader component,<sup>24</sup> the spreadsheet number and the position of its cells are translated as the  $Y$  and  $X, Z$  coordinates, respectively, of each box centre. The value contained in each cell is then interpreted as a factor for each cube's volume, which results in a staggered array of dissimilar boxes (Figure 3(b)). This array can be further refined by using a filter value to remove small cubes.

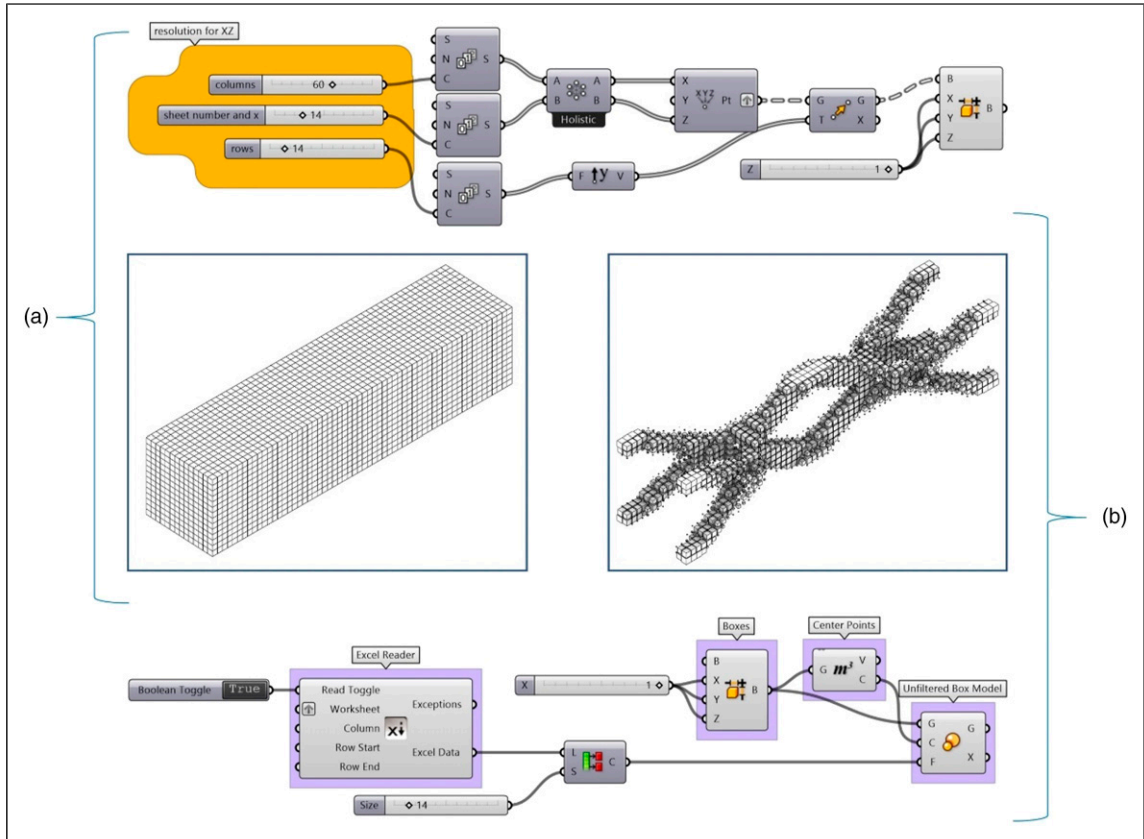


**Figure 3.** (a) Prismatic design domain created in GH using same resolution as in MATLAB and (b) reconstruction of the optimized topology within GH using an Excel reader component.

**Step 2: Definition of a continuum mesh.** To create a continuum polygonal mesh, iso-surfaces are first defined using the MetaBall point charge algorithm, which generates a virtual force field at the centre points of all previous boxes. Each spherical force field is in function of the original density factored by a charge value, which is set to 1 for simplification purposes. To turn these force fields into a continuum mesh, the Cocoon algorithm transforms the iso-surfaces into polygonal meshes.<sup>25</sup> However, the resulting implicit surface still features a staggered mesh. The Dendro smoothing algorithm<sup>26</sup> is thus applied to generate a new even continuum by controlling key filter parameters such as the number and type of iteration, this latter based on either Laplacian or Gaussian method (Figure 4). Depending on the chosen values and types, the continuum's volume can be reduced and the thickness of its elements becoming thinner. However, a drawback with this algorithm is that the definition of the mesh is based on a case-by-case approach, which reads information locally and it does not store the given mesh solution. This leads to asymmetrical distributions of continuum meshes in areas where the original configuration was symmetric. A simple trick to overcome this issue is cutting off the continuum in half – along the symmetrical plane – and mirroring it. The generated volume depends thus on the targeted smooth surface, the deviation of the final volume with respect to the original amount of material and aesthetical preferences.

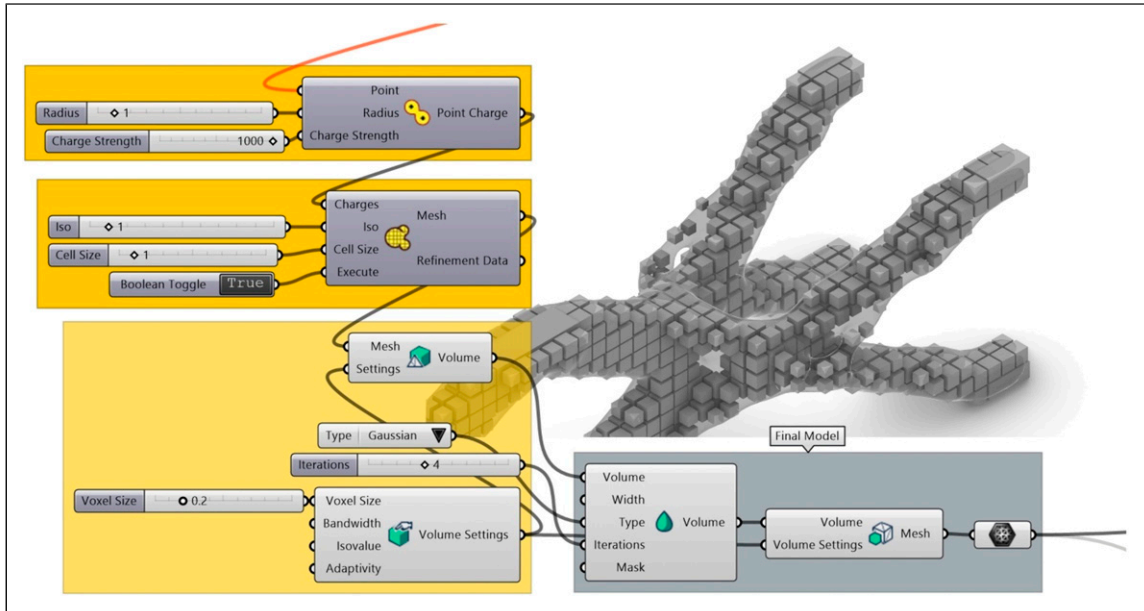


**Figure 4.** Components of the smoothing process: (a) MetaBall Point Charge, (b) Cocoon and (c) Dendro plug-ins.

### Definition of the discrete structures

The definition of the discrete structures takes place in Grasshopper/Rhinoceros environment. Herein, the separation between bar- and node-to-be elements is based on a visual criterion: everything that looks as a linear element, that is, with one axis comparatively longer than the other, will be considered as bar or segment, whereas everything else is considered as node, that is, components where two or more linear elements meet (Figure 5(a)). Once the visual separation is defined, the design procedure of discrete structures consists of two more stages: conversion to regular section bars and design of the connections.

### Conversion to regular section bars

Continuum topology designs feature several bar-like elements with varied cross-sections through their lengths, henceforth, referred as irregular section bars or irregular bars. Since the ultimate goal of the procedure is obtaining equivalent discrete structures using bars with regular sections, yet optimal from a material distribution perspective, the conversion of irregular bars into regular ones should consider how equivalent material distributions affect structural performance. Hence, due to the density-based distribution of forces in the continuum domain, it is valid to assume that such bar elements will experience axial forces, either in compression or tension. However, in some cases, the resulting discrete systems will not display triangular arrays of elements, that is, the system will not be a truss, rising the need of using fixed joints to maintain both global and local equilibrium conditions (Figure 5(b)). These fixed joints will therefore introduce bending moments in the bars, leading to a design controlled by the buckling-resistance of the bars. Consequently, the conversion of an irregular section to a regular section is based on finding equivalent radii of gyration, which establish a relationship between the bending-resistant moment of inertia and the axial strength given by the cross-sectional area of a bar. In fact, the radius of gyration expresses the distance between the centroid of the bar cross-section and the point at which all of the area may be considered as concentrated while having similar

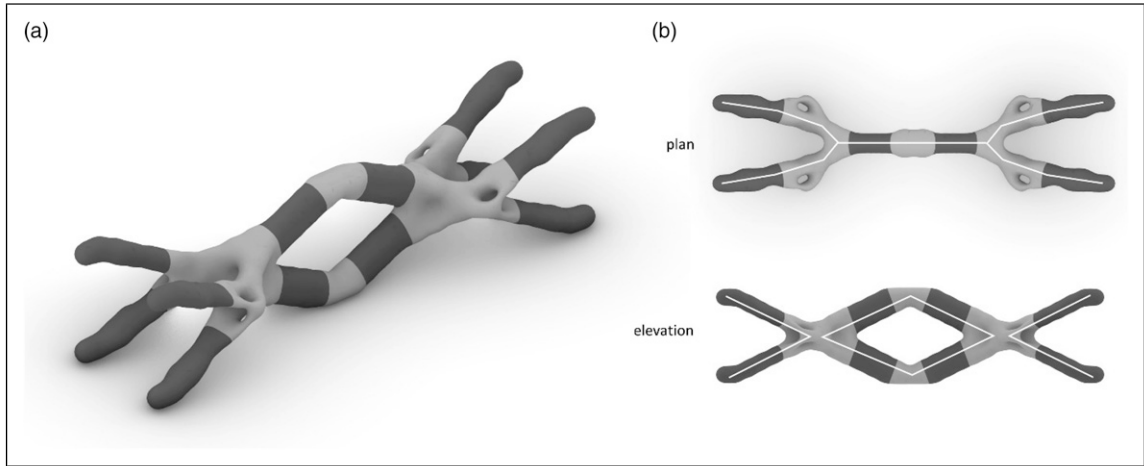


**Figure 5.** (a) Example of a continuum design subdivided into bar- and node-to-be elements and (b) truss vs. frame array of elements in the discrete model.

moment of inertia as the original cross-section. The procedure consists then of three steps: extracting section curves from the mesh continuum model, finding the radius of gyration and determining equivalent regular section.

*Calculation of the area moments of inertia.* After the discrete systems have been defined, the cross-sectional area moments of inertia of each irregular bar must be calculated. According to the theory of mechanics of materials, and provided that the main axis of the bar is aligned to the  $z$  axis (Figure 6), the moments of inertia about  $x$  and  $y$  axes are

$$I_x = \int_A y^2 dA; I_y = \int_A x^2 dA \quad (1)$$

where  $y^2 dA$  and  $x^2 dA$  represent the moments of inertia for the area element  $dA$  about the  $x$  and  $y$  axes, respectively.

*Step 1: Extracting properties of the section curves from the mesh model.* To compute a number of  $[z]$  area moments of inertia, the bar must be subdivided in equidistant segments along the  $z$  axis (Figure 6). This can be done in Rhino or directly in GH. If the computation is to be performed in Rhino, the continuum mesh must be first baked – a single-click action that realizes the mesh within the Rhino environment. If in GH, the selected bar must be converted to a *Brep* (boundary representations). After either action has been performed, the section curves and their properties can be obtained by the following procedure:

- Create mesh planes normal to the main bar  $z$  axis at each point resulting from the subdivision;
- By intersecting each of these planes with the original bar mesh surface, cross-sectional areas are obtained (Figure 7(a));
- Use area moment component to obtain area, centroids, moment of inertia and radii of gyration.

*Step 2: Finding radius of gyration.* In order to compute the radius of gyration, both the area and moment of inertia of a given cross-section must be found. Although custom GH components make the obtention of this



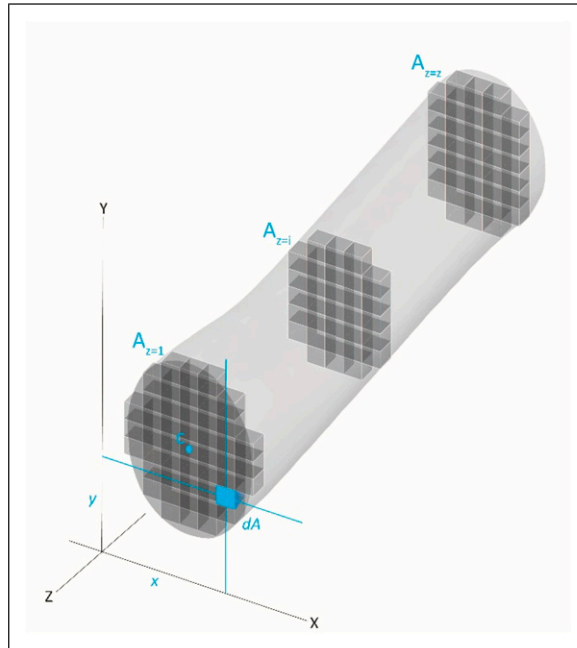


**Figure 6.** Computation of the moments of inertia about  $x$  and  $y$  axes of an irregular bar oriented parallel to  $z$  axis.

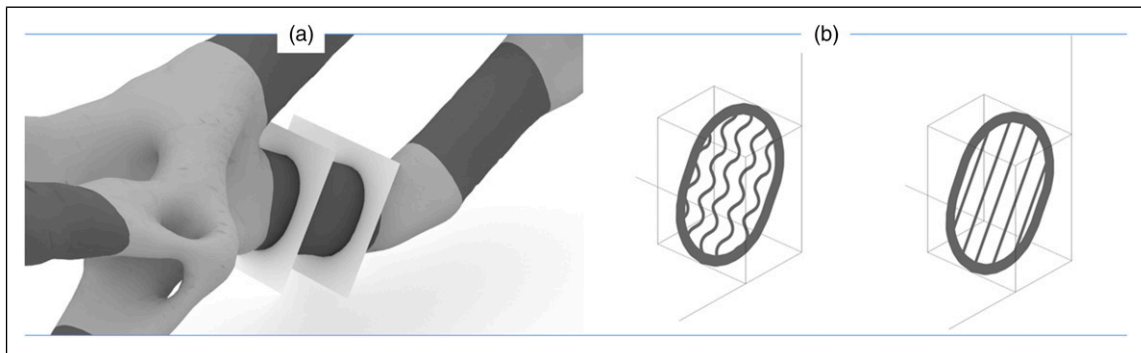


**Figure 7.** (a) Intersecting planar and continuum meshes to determine the cross-section and (b) the equivalent section of a 3D printed bar with gyroid infill.

information relatively straightforward (e.g. area moments), the conversion from irregular to regular sections requires to decide the target type of regular area for the conversion, based on the evaluation of the distribution of material along each axis. Since the material density is assumed homogeneous across the bar, the calculation of the moments of inertia is purely based on geometrical properties. Hence, a variation smaller than 10% of the ratio between moment of inertias about the  $x$  and  $y$  axes ( $I_x/I_y$ ) reveals a quasi-symmetrical cross-section, which can be then turned into a circular cross-section, that is, with radial symmetry. Sections displaying larger variations of the moment of inertias' ratio larger can be converted in regular sections with two lines of symmetry. These types of sections can be formed using two semicircular and one rectangle areas (composite

area) or using an equivalent elliptical area. To account for the influence of the infill density in the mechanical strength of the new regular bars, complementary techniques are required. The approximation method calculation proposed by Li et al.<sup>27</sup> is used to compute the section properties of bars to be printed with gyroid-type of infill (Figure 7(b)). To ensure accuracy of the results, the nozzle size of the 3D printer must be considered when including the shell (a.k.a. wall) thickness and the infill width, whose values are multiples of such size.

*Step 3: Finding equivalent regular section.* In the previous step, the radius of gyration is determined by measuring the area of section curve, the shell thickness and the amount of gyroid infill. Same parameters allow to obtain equivalent radii of gyration of virtually any given shape. However, since the ultimate goal is obtaining standard sections, that is, commercially available, the choices are narrowed down to squares and circular ones. The value of this technique for the purposes of replacing original irregular members by new standard ones is that not only the cross-section is a variable but also the infill percentage and the shell thickness. Thus, for example, a targeted radius of gyration can be achieved by reducing the cross-sectional area and simultaneously increasing the infill percentage, or vice versa.

### Design of connections

In the continuum structure, the nodes are distinguishable only because these are the points where the linear elements change directions. In mathematical terms, if the continuum is understood as a finite curve, the nodes are the points where two consecutive curve segments have different tangents. The advantage is that in this case a node represents a smooth transition from one spatial direction to another. The customization of each linear segment in the discrete version of the structure rises the problem of setting connections between nodes – which remain as in the continuum version – and regular bars. Thus, the design problem is not only about finding a formal transition but one that guarantees a homogeneous distribution of material, that is, stiffness.

### Experimental testing of cylinders

Since the strength capacity of 3D printed elements using common filament materials in combination with different infill percentages was unknown, several tests were performed using  $\varnothing$  10 cm cylinders and length = 20 cm (henceforth referred as  $10 \times 20$  cylinders), printed with PLA, PLA+ and PETG filaments. A second round of tests were performed with  $\varnothing$  8 cm cylinders and length = 16 cm (henceforth referred as  $8 \times 16$  cylinders). The testing machines used for these experiments are targeting concrete specimens, so their capacities are far beyond the expected strength capacity range of the 3D printed cylinders. For this reason, instead of using a compression machine, a flexural testing machine with a capacity of 300 kN was used (Figure 8). Due to its lower capacity, the flexural machine is more accurate in detecting small variations under lower load forces, compared with a conventional compression machine. Preliminary testing of cylinders with varied infill percentages was conducted to determine a capacity threshold ensuring a minimum strength equivalent to 30 kN, that is, 10% of the machine maximum load capacity. This threshold was found to be 20% gyroid infill for all cylinders.

### Results

Figure 9(a) displays the stress–strain relationship of  $10 \times 20$  cylinders under compression, which remains elastic up to 12, 14 and 15 MPa, for PETG, PLA+ and PLA filaments, respectively. Four specimens were tested per each filament. All 12 specimens share similar elastic behaviour and post-yielding behaviour. After yielding, the extension of the plastic response depends on the amount of eccentricity the specimen is able to take. For instance, using PLA produces cylinders that tend to collapse by buckling, losing their strength

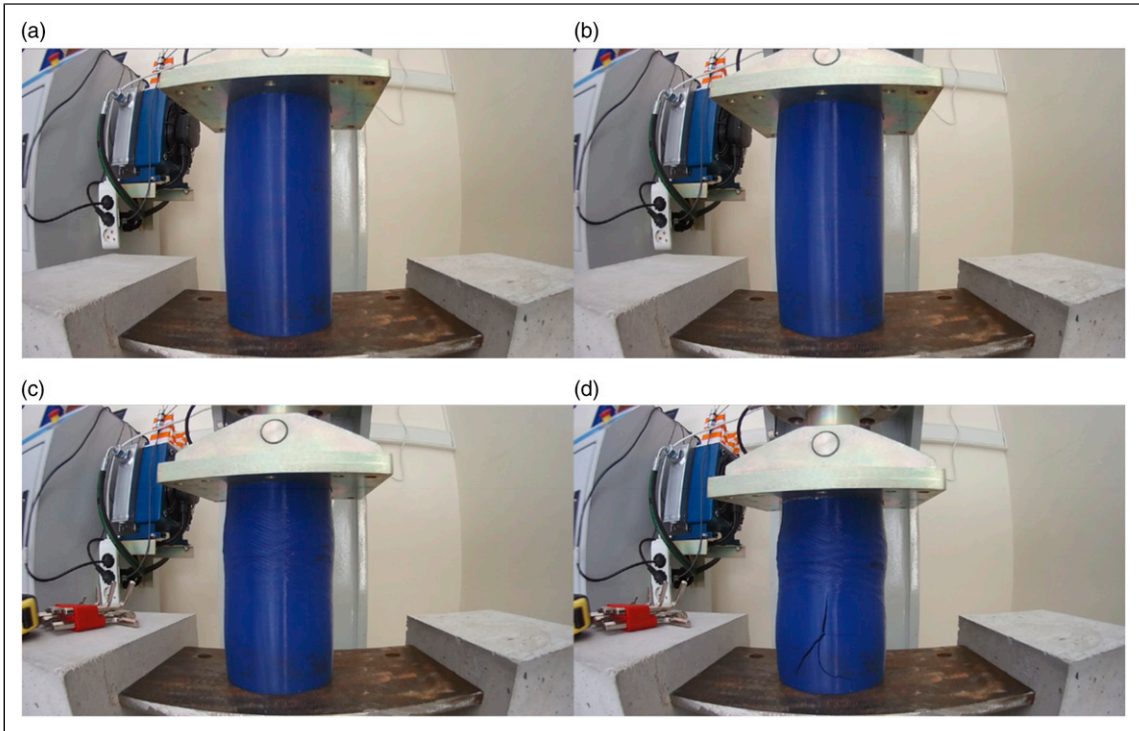


**Figure 8.** Typical compressive testing setup of a 10 × 20 cylinder, 45% gyroid infill PETG: (a) initial loading, (b) initial yielding, (c) post-yield stiffness and (d) stop.

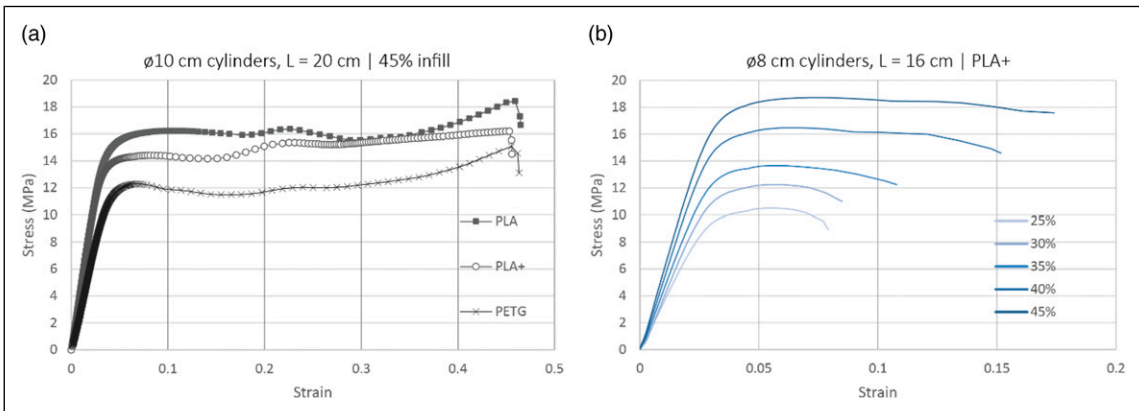


**Figure 9.** Compressive testing results of (a) 10 × 20 cylinders and (b) 8 × 16 cylinders.

capacity earlier than a similar cylinder under pure axial compression. This occurs because of the instability produced by the eccentricity in the loading. When this happens, the test stops. All PLA+ cylinders display a consistent behaviour because the four of them remained stable and seemed to tolerate higher loading eccentricity. Based on the results, it seems clear that the extension of the nonlinear phase of each cylinder depends on the capacity of the material to withstand eccentricity in the loading. Since eccentricity in compressive-only members entails tensile stresses acting on the exposed side of the curve, the lack of stability of both PETG- and PLA-based cylinders can be attributable to an unbalanced distribution of compressive-tensile strength in these materials. Although the difference between cylinders made of PLA+ and the other ones may be related to variations due to the printing process, the small difference flexural-tensile strength of the PLA+, 75 vs. 65 MPa, respectively, suggests that this material has a balanced distribution of the tensile-compressive stress and hence it is more suitable for structural applications involving elements subjected to different type of loading.

A setback with the  $10 \times 20$  cylinders was their weight, which was around 0.92 kg per specimen, rising doubts of the practical use of 45% gyroid infill. For this reason, a new round of testing was conducted with  $8 \times 16$  cylinders, made of PLA+, and with different infill percentages. The results (Figure 9(b)) display an increased strength for a 45% infill  $8 \times 16$  cylinder with respect to a  $10 \times 20$  cylinder with equal infill percentage, 17 vs. 14 MPa, respectively. This can be attributable to the reduced effect of buckling in the shorter cylinder. In addition, the graph shows that the extension of the post-yielding capacity of a cylinder is proportional to the amount of infill it has. The weight of a 45%  $8 \times 16$  cylinder is about 0.5 kg, whereas a 25% one weights about 0.3 kg.

## Design and hybrid fabrication of discrete prototypes

To test the proposed method, a cantilever beam was first topology optimized in MATLAB and then reinterpreted in GH (Figure 10). The initial design domain mesh contained  $90 \times 30 \times 14$  FE, and thus for the purposes of fabrication, similar dimensions in centimetres were considered for the initial prototypes.

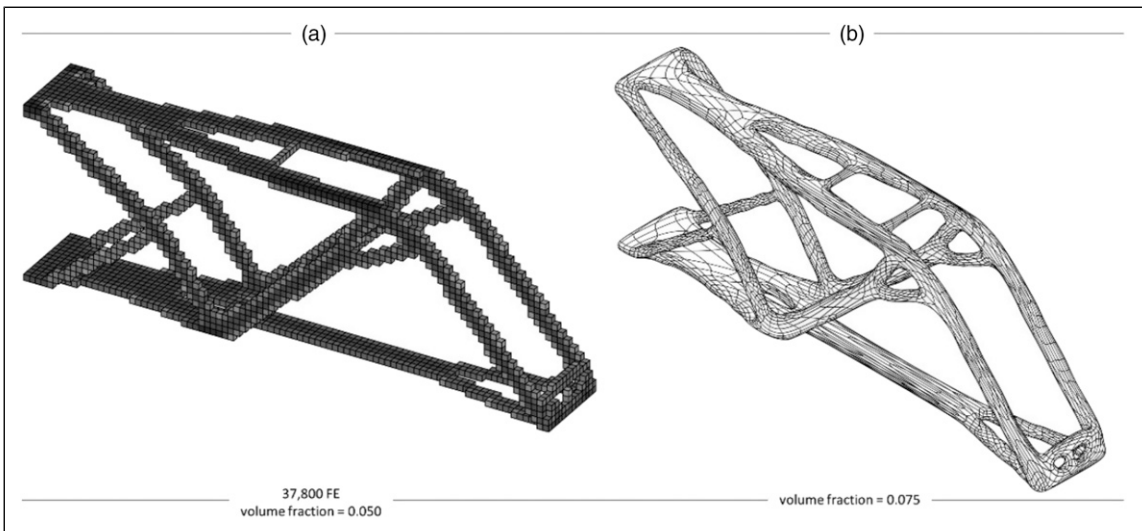


**Figure 10.** Continua topology optimization (a) as defined in MATLAB and (b) as reinterpreted in GH

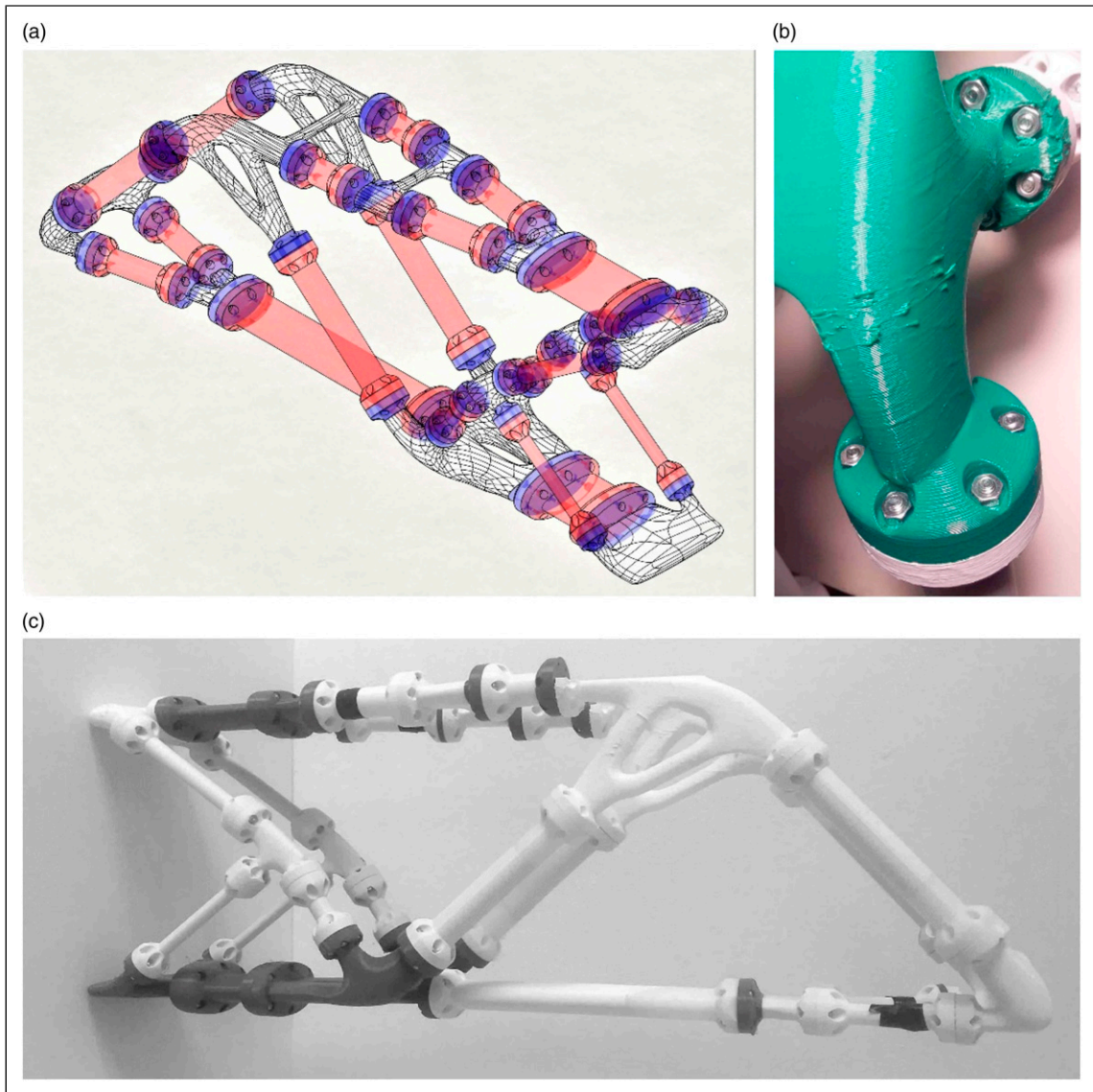


**Figure 11.** (a) Computational model, (b) a 6-screw connection with circular slots for bolts and (c) discrete PLA cantilever prototype.

### *Polylactic acid+ prototypes*

Before combining different materials, two preliminary cantilever prototypes were designed and built using only 3D printed components, in order to learn from the experience of assembling discrete elements. Using the radii of gyration, the irregular bars of the continuum were converted into bars with circular or ellipsoid sections. Here, the goal was using equal infill percentage for both regular and irregular components. For this reason, diameter of sections and shell thicknesses were modified to obtain equivalent values between radii of

gyration. Although the discretization of the original continuum shape is straightforward, from a design point of view, the critical part are the connection points. Due to the bending moment developed at the nodes, connections require to be rigid and thus, a larger contact surface was provided and bolted at the perimeter. Since the bars were printed with circular or ellipse sections, the logic choice seemed to be an also circular connecting plate. For assembling the first 20% gyroid infill PLA prototype (Figure 11(a)), six  $\varnothing$  4 mm bolts were used (Figure 11(b)).

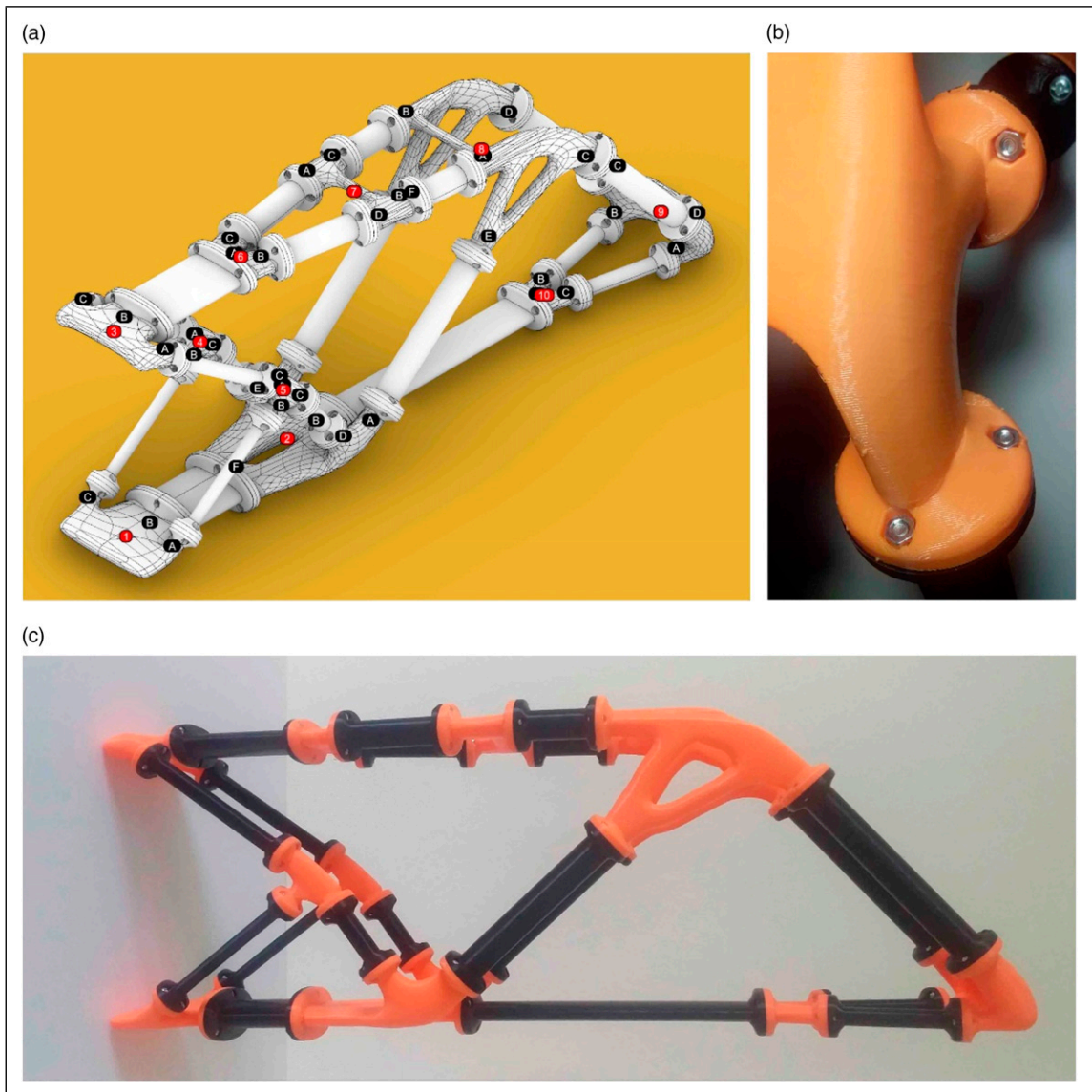


**Figure 12.** (a) Computational model, (b) a 3-screw connection with hexagonal slots for bolts and (c) discrete PLA+ cantilever prototype.

The reason for using  $\varnothing 4$  mm bolts is their wide use and availability in the local stores. However, due to the number of connections, the bolts and nuts represented about 20% of the total weight of final model. In addition, some of the bolts could not be fitted in due to the curvature of the organic parts. For this reason, a new version of the cantilever was designed (Figure 12(a)), including connections with only three bolts and thinner plates (Figure 12(b)). Further improvements include the modification of the notch that receives the hexagonal nut, to easy the screwing process. This second version was printed in PLA+ with similar infill percentage.

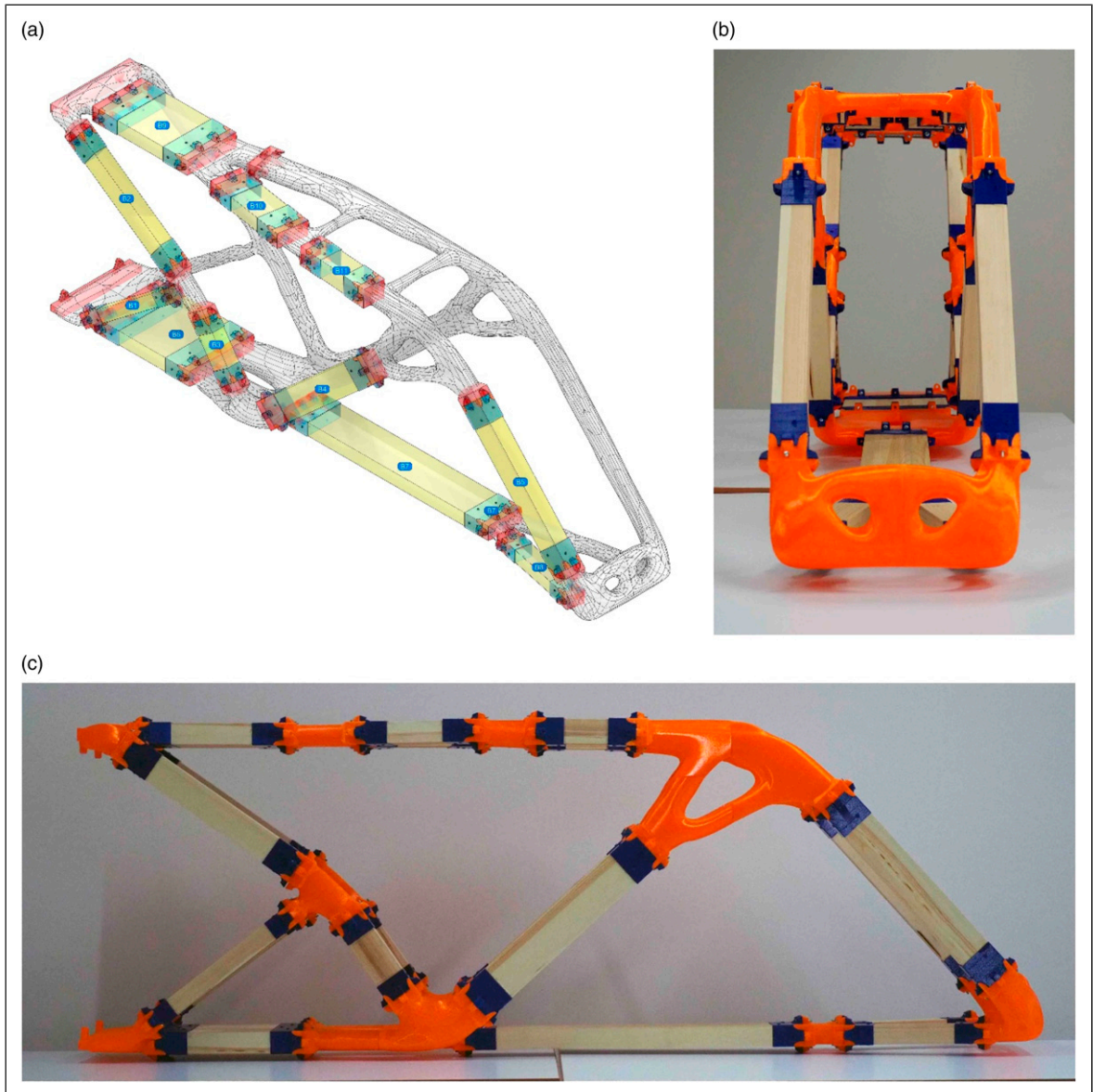


**Figure 13.** (a) Computation model showing only some of the bars for simplification, (b) front and (c) side view of the hybrid prototype.

### Hybrid timber + polyethylene terephthalate glycol prototype

To explore the advantages of the method when fabricating real scale structures, a new 180 cm × 60 cm × 28 cm cantilever prototype was designed and built. This hybrid prototype (Figure 13) comprised 3D printed PETG parts connecting 19 timber bars of varied cross-sections, made of Siberian Pine – a type of wood commonly available in Turkey. The choice of combining these two materials partially responded to the first author’s previous experiences combining timber battens and PLA nodes for the design of full-scale gridshells. In terms of material strength, pine wood bars were always stronger than the PLA nodes, and since bar length was restricted to be <1 m, bars had also larger bending capacity, leading to cracks in the nodes. Another issue was that commercial pine wood usually presented knots, which might lead to local structural weakness if used in a full-scale structure, because of the bar elements becoming larger. For these reasons, PETG and Siberian Pine were chosen for the current hybrid prototype due to their similar flexural strengths, which are 68 and 65 MPa,<sup>28</sup> respectively.

*Design of the nodes.* Whereas in the previous prototypes, the printed bars had circular cross-sections; in the hybrid version, the timber bars featured a rectangular cross-section. This decision was based on the easiness of production and assembling. By means of the radii of gyration, equivalent cross-sections were determined for each timber bar. However, the new section shape demanded a slightly different approach when designing the connecting plates as these elements must transfer stress from rectangular sections to a section that resembles an ellipse or a circle. The design of the connection was also based on the first author’s previous experiences

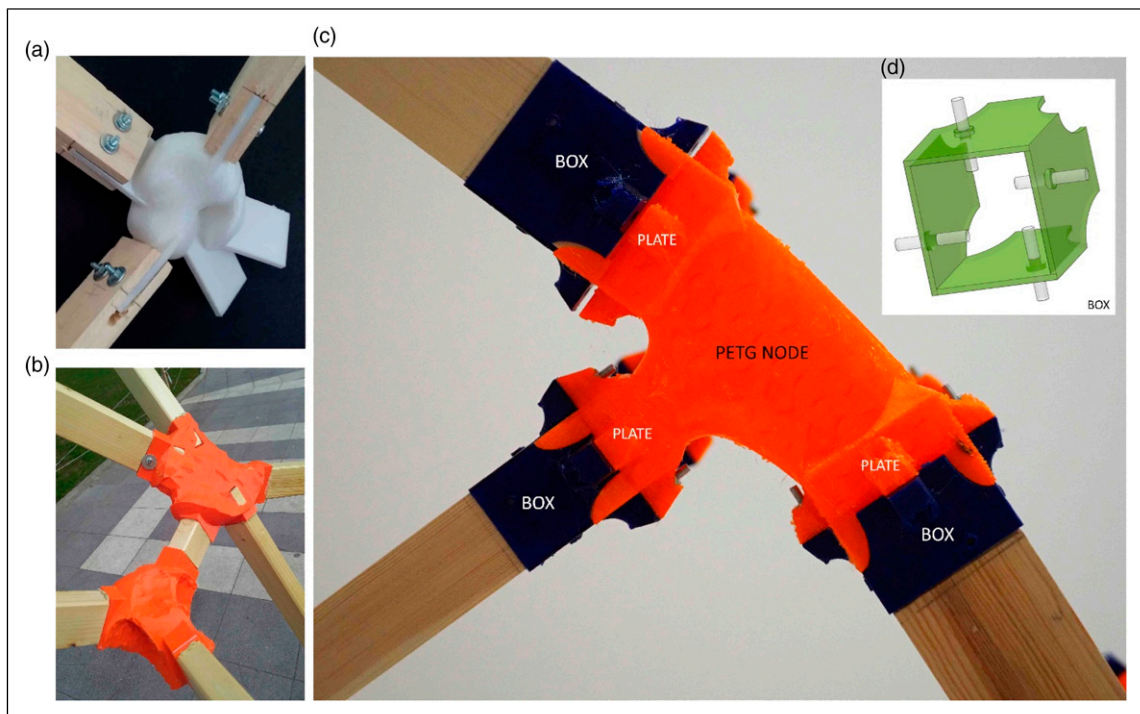


**Figure 14.** Previous works with PLA+ and pine wood: (a) node inserted in the timber bars, (b) timber bars inserted in the nodes, (c) close-up of a 3-bar node in the hybrid prototype and (d) detail of the PETG box to be attached at the end of each bar.



with hybrid fabrication of full-scale prototypes. In an early gridshell structure, and following similar studies,<sup>29</sup> the PLA+ nodes were designed with additional 5 mm plates to be inserted in the 20 mm × 50 mm pine battens and pinned by two screws (Figure 14(a)). Although this connecting method made the structure easy to assemble, plates were also easily broken. Thus, for the design of the next gridshell structure, a rather rigid connection was proposed: hollowed rectangular prisms were inserted in the nodes to receive the concurrent wooden battens (Figure 14(b)). While these connections increased the general stiffness of the structure, the rigid connections made difficult the assembly of the last bars of the structure, resulting in some broken nodes due to the excessive forces applied when manipulating the bars.<sup>30</sup> In the hybrid prototype, the design of the nodes was based on the lessons learnt: the nodes must allow the connected members to be inserted into and removed from the structure with easiness, and the nodes should be strong regardless of the direction of the layers in which they are printed.<sup>30</sup> For this reason, each connection consists of two elements: the bar's box surrounding the concurrent bar, glued and screwed to the timber, and the receiving plate connected to the 3D printed section, including stiffeners at each corner (Figure 14(c)). These two parts were assembled by  $\varnothing$  4 mm bolts, whose number depends on the regularity of the section: four bolts for square sections (Figure 14(d)) and six or eight bolts for rectangular ones.

## Discussion and concluding remarks

From a methodological point of view, the reinterpretation of the FE mesh within GH requires a new definition of constraints for the optimization. For example, the algorithms that produce continuum polygonal mesh iso-surfaces read the data at local level and thus produce different results for similar array, leading to asymmetries in the reconstruction of the continuum. This will lead to variation in the volume of material used in the final design, although opens up the possibility of visual manipulation based on simple aesthetical criteria (Figure 15). The best example of this is the visual-based separation between bar- and node-to-be elements during the discretization phase. In addition, a conversion method based on the radius of gyration facilitates matching an irregular section to virtually any possible section shape. The fact that a targeted radius of gyration can be achieved by reducing the cross-sectional area and simultaneously increasing the infill percentage opens up to the use of any standard section members by controlling the infill percentage of the component.

From a practical point of view, the keystone of the discretization process lies in the design of the nodes. Thus, the design problem is not only about finding a shape transition between discrete members but one that guarantees a homogeneous distribution of material, that is, stiffness. In this regard, the main advantage of a discrete 3D printed structure over a continuum one is that layer deposition can be controlled in a piece-by-piece approach, and thus ensuring that layers are printed normal to the direction of the main force, which is usually perpendicular to the  $z$  axis. In the study described in this article, the authors followed an empirical approach when designing the nodes and increasing the cross-sections of bars and nodes in the region close to the connections to guarantee (i) a reduction in the axial stress, (ii) a balance in the distribution of material density (avoiding stress concentrations due to the holes) and (iii) a transfer of bending moment (if any). However, further research is needed to optimize the material distribution of the nodes while ensuring the fulfilment of the conditions aforementioned. In this regard, ad-hoc GH plug-ins such as Millipede<sup>31</sup> or OptiStruct (as described in the study of Prayudhi<sup>29</sup>) could provide the correct interface for these localized optimizations.

In practice, the conversion from irregular to regular section bars is based on controlling the desired dimensions. This is because the topology optimization is based on a linear distribution of stiffness to reduce displacement under certain loading conditions. Stiffness in this context is a measure of density. That is why the distribution of material in each FE represents the amount of forces that element is bearing. The density is displaying the way forces are distributed. Hence, by equalizing the moment of inertia of different sections, the targeted density remains unaltered and, by extension, the load path remains the same. However, by dividing

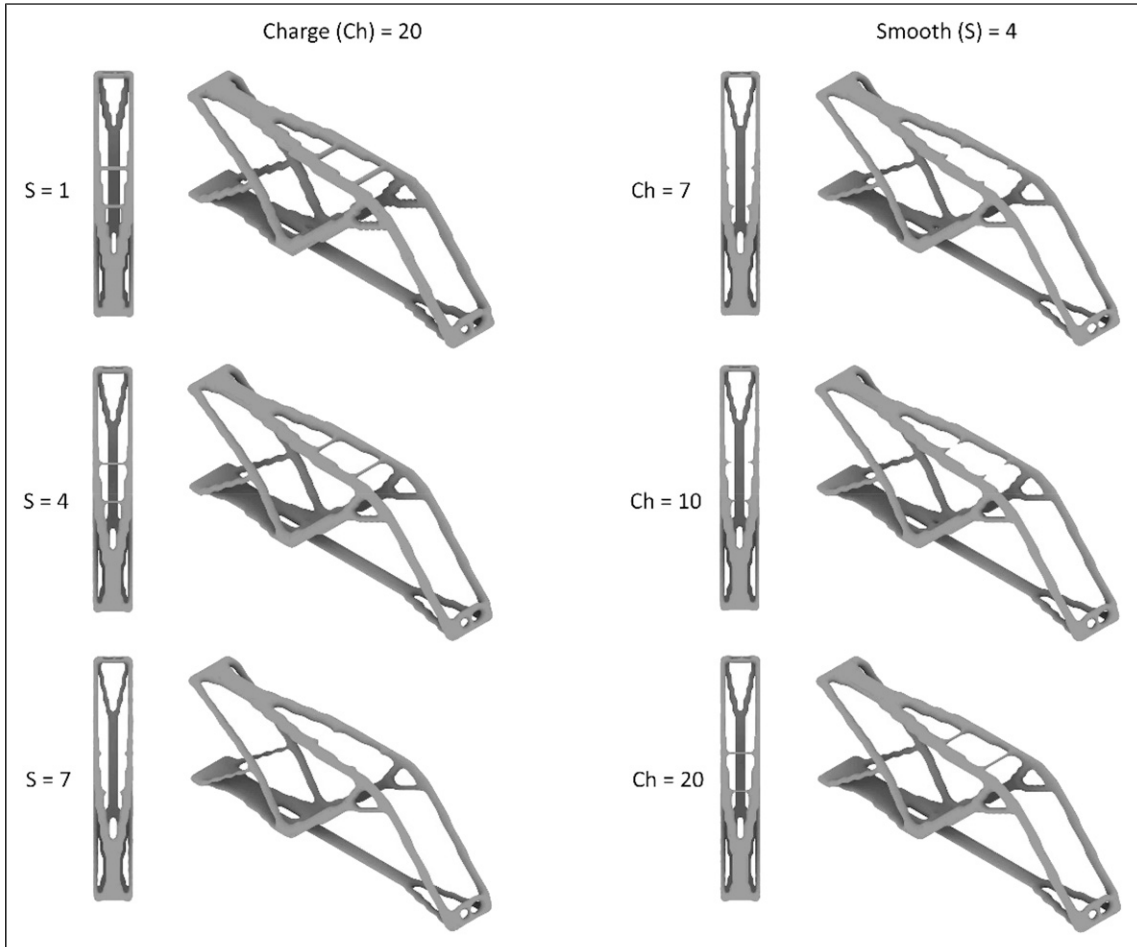


**Figure 15.** Influence of the charge and smoothing values in the final continuum mesh and the volume fraction.

the continuum system into discrete elements, such path of distributed forces is interrupted. In order to restore it, additional elements for connections must be added and thus, increasing the available density, a.k.a. stiffness, at a local level. A further research could address the implications of such additional stiffness, by comparing the node/bar stiffnesses and thus determining whether connections should be stronger or weaker than the bars.

Future applications of the work presented in this study can be related to both the design procedures and hybrid fabrication. In terms of computational implementations, since the procedure described here is complementary to a MATLAB-based method,<sup>23</sup> further studies may propose a sole GH-based algorithm, relying on the use of current available plug-ins (e.g. Millipede). This approach may simplify the data conversion (done through spread sheets in this study) and benefit from including fabrication constraints into the topology optimization. In the case of the geometrical characterization of the 3D printing material, however, this will challenge the density approach of the topology optimization, as in 3D printing ‘the specimen is actually a structure, not a material’.<sup>15</sup> Hence, if successfully determined, a comprehensive topology optimization would yield designs that are not only optimal from a material savings’ perspective but

also increasing the mechanical strength of the 3D printed pieces. In terms of hybrid fabrication, the mixture of materials can be extended to other common sources, such as steel profiles and carbon fibre polymers. Given the high modulus of elasticity of the steel, bar sections can be further reduced, increasing the potential for the achievement of high strength lightweight structures, but challenging the design of the connections with carbon fibre nodes. Similarly, given the regular nature of the applied commercial bars (whether timber or steel-based), straight components may be used as supports for 3D printing the nodes, leading to the use of temporary structures supporting the bars, which later can be removed. Such approach would allow to adjust the printing direction to that of major convenience, from a structural strength point of view.<sup>11,20</sup>

## Acknowledgments

The authors would like to thank Dr. Mert Yücel Yardımcı for his helpful guidance on the test settings and Ceren Duyal for her kind help with the testing instruments.

## Declaration of conflicting interests

The author(s) declared no potential conflicts of interest with respect to the research, authorship, and/or publication of this article.

## Funding

The author(s) disclosed receipt of the following financial support for the research, authorship, and/or publication of this article: The work presented in this paper was funded by Yaşar University Project Evaluation Commission (PDK) with the project BAP078 “Exploring additive manufacturing technologies for the realization of continuum and discrete topology optimized structures”.

## ORCID iD

Mauricio Morales-Beltran  <https://orcid.org/0000-0003-4883-4314>.

## References

1. Rozvany GIN. A critical review of established methods of structural topology optimization. *Struct Multidiscip Optim* 2009; 37(3): 217–237. DOI: [10.1007/s00158-007-0217-0](https://doi.org/10.1007/s00158-007-0217-0).
2. Bendsoe MP and Sigmund O. *Optimization of structural topology, shape, and materials*. Heidelberg, Germany: Springer, 1998.
3. Deaton JD, Grandhi RV. A survey of structural and multidisciplinary continuum topology optimization: Post 2000. *Struct Multidiscip Optim* 2014; 49(1): 1–38. DOI: [10.1007/s00158-013-0956-z](https://doi.org/10.1007/s00158-013-0956-z).
4. Mostafavi S, Morales-Beltran M and Bioria N. Performance driven design and design information exchange. In: 31st International Conference on education and research in Computer Aided Architectural Design in Europe eCAADe (eds R Stouffs and S Sariyildiz), pp. 117–126. Delft, The Netherlands: Delft University, 2013.
5. Aage N, Amir O, Clausen A, et al. Advanced topology optimization methods for conceptual architectural design. In: P Block, J Knippers, NJ Mitra, et al. (ed) *Advances in Architectural Geometry 2014*. Cham, Switzerland: Springer International Publishing, 2015, 159–179.
6. Stromberg LL, Beghini A, Baker WF, et al. Topology optimization for braced frames: Combining continuum and beam/column elements. *Eng Struct* 2012; 37: 106–124.
7. Allahdadian S, Boroomand B and Barekatein AR. Towards optimal design of bracing system of multi-story structures under harmonic base excitation through a topology optimization scheme. *Finite Elem Anal Des* 2012; 61: 60–74.
8. Dapogny C, Faure A, Michailidis G, et al. Geometric constraints for shape and topology optimization in architectural design. *Comput Mech* 2017; 59(6): 933–965. DOI: [10.1007/s00466-017-1383-6](https://doi.org/10.1007/s00466-017-1383-6).

9. Søndergaard A, Amir O, Eversmann P, et al. Topology Optimization and Robotic Fabrication of Advanced Timber Space-Frame Structures. Reinhardt D, Saunders R and Burry J (ed). *Robotic Fabrication in Architecture, Art and Design 2016*. Cham, Switzerland: Springer International Publishing, 2016, 190–203. DOI: [10.1007/978-3-319-26378-6\\_14](https://doi.org/10.1007/978-3-319-26378-6_14).
10. Dickson AN, Abourayana HM and Dowling DP. 3D printing of fibre-reinforced thermoplastic composites using fused filament fabrication—A review. *Polymers* 2019; 12: 2188.
11. Yao T, Zhang K, Deng Z, et al. A novel generalized stress invariant-based strength model for inter-layer failure of FFF 3D printing PLA material. *Mater Des* 2020; 193: 108799.
12. Elkaseer A, Schneider S and Scholz SG. Experiment-based process modeling and optimization for high-quality and resource-efficient FFF 3D printing. *Applied Sci* 2020; 10: 2899.
13. Shaqour B, Abuabiah M, Abdel-Fattah S, et al. Gaining a better understanding of the extrusion process in fused filament fabrication 3D printing: a review. *Int J Adv Manuf Technol* 2021; 114(5): 1279–1291. DOI: [10.1007/s00170-021-06918-6](https://doi.org/10.1007/s00170-021-06918-6).
14. Fernandez-Vicente M, Calle W, Ferrandiz S, et al. Effect of infill parameters on tensile mechanical behavior in desktop 3D printing. *Addit Manuf* 2016; 3(3): 183–192. DOI: [10.1089/3dp.2015.0036](https://doi.org/10.1089/3dp.2015.0036).
15. Mazzanti V, Malagutti L and Mollica F. FDM 3D printing of polymers containing natural fillers: A review of their mechanical properties. *Polymers* 2019; 11(7): 1094.
16. Decuir F, Phelan K and Hollins BC. Mechanical strength of 3-D printed filaments. In: 32nd Southern Biomedical Engineering Conference (SBEC), Shreveport, LA, 11–13 March, 2016, 2016,47–48.
17. Mostafavi S, Kemper BN, Du C. Materializing hybridity in architecture: design to robotic production of multi-materiality in multiple scales. *Archit Sci Rev* 2019; 62(5): 424–437. DOI: [10.1080/00038628.2019.1653819](https://doi.org/10.1080/00038628.2019.1653819).
18. Mathworks. MATLAB R2016b, 2016.
19. McNeel R. Rhinoceros 3D, 2016. Available from: <https://www.rhino3d.com/>.
20. Ahn S, Montero M, Odell D, et al. Anisotropic material properties of fused deposition modeling ABS. *Rapid Prototyp J* 2002; 8(4): 248–257. DOI: [10.1108/13552540210441166](https://doi.org/10.1108/13552540210441166).
21. Dizon JRC, Espera AH, Chen Q, et al. Mechanical characterization of 3D-printed polymers. *Addit Manuf* 2018; 20: 44–67. Available from: <https://www.sciencedirect.com/science/article/pii/S2214860417302749>.
22. Dong Y, Milentis J and Pramanik A. Additive manufacturing of mechanical testing samples based on virgin poly (lactic acid) (PLA) and PLA/wood fibre composites. *Adv Manuf* 2018; 6(1): 71–82. DOI: [10.1007/s40436-018-0211-3](https://doi.org/10.1007/s40436-018-0211-3).
23. Liu K and Tovar A. An efficient 3D topology optimization code written in Matlab. *Struct Multidiscip Optim* 2014; 50(6): 1175–1196. DOI: [10.1007/s00158-014-1107-x](https://doi.org/10.1007/s00158-014-1107-x).
24. Miller N and Proving G. Lunchbox for Grasshopper [Internet], 2020. Available from: <https://www.food4rhino.com/app/lunchbox>.
25. Stasiuk D. Cocoon [Internet], 2015. Available from: <http://www.bespokegeometry.com/2015/07/22/cocoon/>.
26. Eclrlabs. Dendro [Internet], 2018. Available from: <https://www.eclrlabs.com/dendro/>.
27. Li D, Dai N, Jiang X, et al. Density aware internal supporting structure modeling of 3D printed objects. In: International Conference on Virtual Reality and Visualization, Nanchang, China, 17–20 October, 2021. ICVRV, 2015, 209–215.
28. Jankowska A, Boguslaw A and Mastyna B. Characteristic technical properties of Siberian yellow pine (*Pinus sibirica* Du Tour.) wood. *Sylvan* 2017; 161(9): 756–762.
29. Prayudhi B. 3F3D: Form follows force with 3D printing. MSc Thesis, Delft University of Technology, Delft, 2016.
30. Morales-Beltran M, Karatepe E, Çetin K et al. Hybrid materiality: Combining digital and analogue fabrication in the design of a freeform gridshell structure. *Int J Digit Innov Built Environ* 2021; 10(2): 46–62, doi:[10.4018/IJDIBE.2021070104](https://doi.org/10.4018/IJDIBE.2021070104).
31. Michalatos P. Millepede [Internet], 2014. Available from: <http://www.sawapan.eu>.